Journal Article

A comparison of the magnetic properties of Ni and Co nanowires deposited in different templates and on different substrates

Yalcin, O., Kartopu, G., Cetin, H., Demiray, A.S. and Kazan, S.

A comparison of the magnetic properties of Ni and Co nanowires deposited in different templates and on different substrates

O. Yalçın[1,*] , G. Kartopu[2], H. Çetin[3], A. S. Demiray[4], S. Kazan[4]

[1]*Department of Physics, Niğde University, 51240 Niğde, Turkey*
[2]*Centre for Solar Energy Research (CSER), GlyndŵrUniversity, OpTIC, St. Asaph Business Park, St. Asaph, LL17 0JD, UK*
[3]*Department of Physics, Bozok University, 6600 Yozgat, Turkey*
[4]*Department of Physics, Gebze Institute of Technology, 41400 Gebze Kocaeli, Turkey*

Abstract

Nickel (Ni) and cobalt (Co) nanowire arrays (NWs) grown by electrodeposition in porous nano-templates are studied by ferromagnetic resonance (FMR) technique at room temperature (RT) by comparing the effects of template type (alumina and polycarbonate) and the deposition substrate (i.e. metallic back contact). The line-width and resonance field of the FMR spectra strongly depended on the orientation of the applied field direction. A model is developed to analyze the spectra in order to extract the magnetic parameters such as *g*-values, spin-spin relaxation times (T_2) and uniaxial anisotropy parameters. The experimental FMR spectra and their resonance field values were fitted using the imaginary part of magnetic susceptibility and a dispersion relation of magnetization, including the Bloch-Bloembergen type damping term. The easy axes of magnetization for all Ni and Co NWs were found to be perpendicular to the wire-axis. Surface spin modes have been observed only when pure Au was used as substrate. A discussion will be provided to explain the observed differences in terms of the anisotropic behaviour and magnetic parameters of the NWs for different substrates and growth templates.

Keyword(s): Magnetic nanowires, Ferromagnetic resonance, Magnetic anisotropy

*Corresponding author. Phone.: +90 388 2254068; fax: +90 388 2250180.
E-mail: o.yalcin@nigde.edu.tr , orhanyalcin@gmail.com (O. Yalçın).

1. Introduction

The magnetic NWs are now a popular class of magnetic nanostructures [1]. The NWs have been receiving steadily increasing attention in various disciplines, including biology, spintronics, biomedicine, chemistry and physics due to their various potential applications, for example, thermoelectric nanowires, bio-sensors, computer hard disks, microwave electronics devices, nano-transistors, nanorobots, photodetectors, solar cells, photonic band gap materials, metallic screens, etc. [2-4]. Nickel NWs in particular are applied to new technologies such as plasmonic resonance sensors, negative permeability, optical sensing, perpendicular magnetic storage media and wire-grid type micro polarizer, and to fabricate single-nanowire based functional devices [5, 7-14]. These structures are also used as building blocks in high-throughput screening, lab-on-a-chip, trenches and capacitors in integrated circuits [5]. Compared to bulk magnetic materials, magnetic NWs offer additional degrees of freedom associated with their shape anisotropy and properties that are controllable, e.g. the array packing density and wire diameter and length. On the other hand, as the dimensions of materials decrease from bulk to the nano structure the surface effects come to play, emerging in new and interesting properties [6].

Co and Ni NWs are usually deposited by electrodeposition [7, 15-28], tetra-ethylene glycol reduction process [29] and sequential pulsed laser deposition [30]. Current–voltage measurements [31], applied via the scanning tunnelling spectroscopy in constant height and constant current mode [32-33], revealed superconducting properties of ferromagnetic Co NWs [34]. The interaction force [35], nuclear spin-lattice relaxation [36], the effects of the solution pH (on wire growth and properties) [37] and magnetic torque characterization [38] were also reported for Co NWs [33, 39-40]. The origin of easy-axes of magnetization has been studied for various magnetic NWs [16, 7, 41-44].

FMR experiments have been performed for some ferromagnetic NWs so far [45-51]. The FMR technique has proved to be a very powerful technique [52-60] in providing information on the magnetization, magnetic anisotropy and relaxation times, as well as the damping in magnetization dynamics and the spin wave resonance (SWR) [61-66]. The substrate effects on magnetic properties of electrodeposited magnetic NWs have also been reported. For example, Co/Cu multilayer NWs fabricated into anodic aluminium oxide templates using Ag and Cu

substrates and direct–current (dc) electrodeposition were studied in Ref. 67. Template effects for anisotropy of NWs are reviewed in Ref. 68. However, the effects of using different substrate and template types on spin wave modes have not been studied to date.

In this article, we report on the effects of using different substrates and nano-templates on the spin wave modes of Co and Ni NWs as observed at the RT. The magnetic properties of Co and Ni NWs with the easy axis along perpendicular direction have been analyzed with respect to varying packing factor (P) and aspect ratio (τ) of the wires. The spin wave modes when using single Au layer and Cu/Au bilayer substrates were investigated in detail in the frame of theoretical calculations.

2. Experimental Procedures

Ni and Co NWs were prepared by dc electrodeposition inside the pore channels of 45 μm thick commercial (Whatman anodisc) alumina (AAO) and polycarbonate (PCTE) membrane films having 200 nm (nominal) diameter pores . The deposition procedure followed the method described in Refs. 69-71. Briefly, a conformal metal film was first coated on one side of the membrane (to serve as the working electrode) using either a single layer of ~50 nm sputter-deposited Au film or a thin Au film (≤50 nm) followed by a supporting thick layer (~1000 nm) of electrodeposited Cu film (Fig. 1, steps 1 and 2). It was noted that template pores were not well sealed using the single Au film. With the Cu support the template surface was uniformly covered and all the pores were sealed with some out-growth into the pores observable (as illustrated in Fig. 1). In order to prevent the deposition of a magnetic thin film on the back of the working electrode (i.e. the metal substrate), an insulating layer of nail polish was applied onto this surface. The template was then mounted in an electrochemical cell with the pore channels wetted with deionised water via ultrasonic agitation prior to NWs deposition. The NWs were then electrodeposited (Fig. 1, step 3) in a conventional three-electrode configuration applying -1.2 V was applied (vs. Ag/AgCl reference electrode) between the sample and a Pt counter-electrode through an aqueous electrolyte, containing 100 g/L Ni or Co sulphate and 50 g/L boric acid (pH=3). The wire length was adjusted to ≥15 μm to obtain high aspect ratio NWs. To assess the template filling ratio and the microstructure using this procedure, the template was removed either by chemical etching (for PCTE samples) or mechanical polishing (for AAO samples). In the case of AAO templates the unfilled portion of the template was carefully grinded until the wire tips were exposed which

was followed by ultrasonic cleaning. In all cases, extremely high filling rates (>90%) were achieved. Figure 1 exhibits typical geometry of such specimens.

The FMR spectra of the thus prepared (embedded) Ni and Co NWs were collected by an X-band (~9.8 GHz) Bruker EMX spectrometer at RT. A goniometer has been employed to rotate the sample around the wire axis. Anisotropic spectra have been recorded at different angles of excitation with respect to the film plane, in order to attest sample homogeneity (magnetic or structural) and to deduce the magnetic parameters.

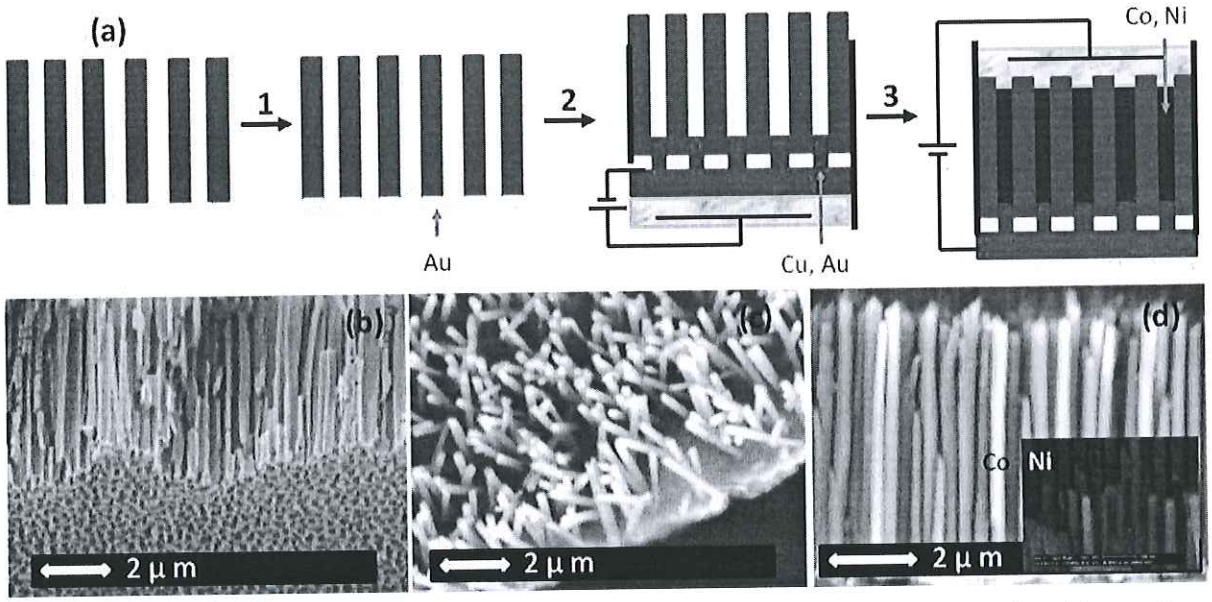

Fig.1. (**a**) Schematic representation of magnetic nanowire deposition. (1) Au thin film sputter deposition on the template, (2) Complete sealing of the pores by Cu electrodeposition, and (3) Co/Ni electrodeposition for the bottom-up growth of ferromagnetic NWs inside the pore channels. (**b**) An AAO template (~200 nm pore diameter) in two-dimensional arrangement, (**c**) Cross-section Co NWs deposited inside PCTE pore channels. (**d**) Cross-section Co NWs (Ni, inset) deposited inside AAO pore channels.

3. Theoretical Model

To extract the magnetic parameters and resonance fields the following theoretical model was used. The experimental and theoretical coordinate systems for the *dc* magnetic field $\vec{H}$, relative orientation of equilibrium magnetization $\vec{M}$ and the geometric factors of the hexagonal arrangement of NWs were considered as depicted in Fig.2.

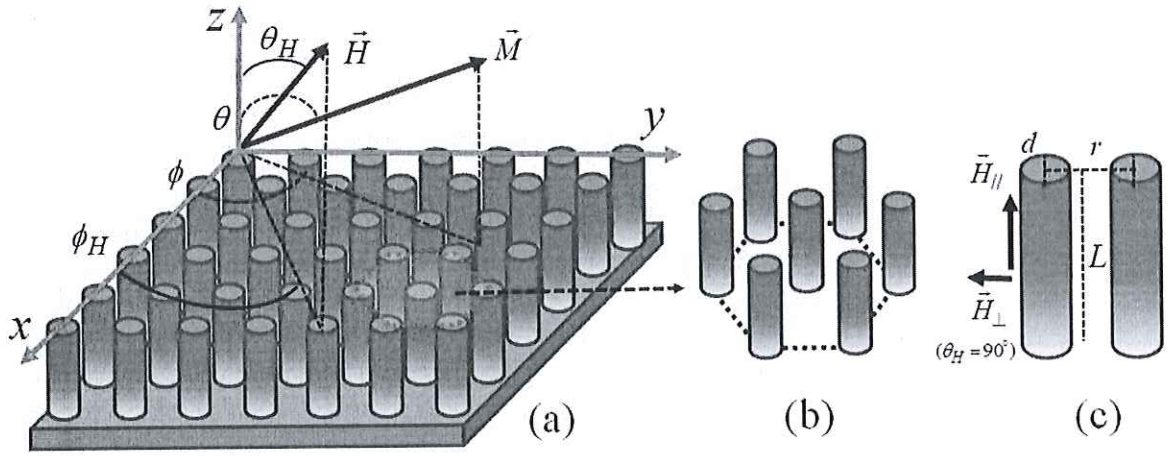

Fig. 2. (**a**) Schematic representation of the magnetic NWs and the relative orientation of the equilibrium magnetization ***M*** and the dc component of the external magnetic field ***H*** considered for the FMR experiments and their theoretical calculations. (**b**) Close-up view of a hexagonal nanowire array (dashed lines indicate the six fold symmetry around the central wire). (**c**) Geometrical parameters used in the calculation of the packing factor *P*.

The free-energy density equation for homogeneously magnetized NWs films can be written as

$$E = -\vec{M}\cdot\vec{H} + K_{eff}\sin^2\theta\,, \tag{1}$$

where the first term corresponds to Zeeman energy, with the second term representing the effective anisotropy energy [72-74]. Here, (θ,ϕ) and (θ_H,ϕ_H) are angles in spherical coordinates for $\vec{M}$ and $\vec{H}$, respectively, while $K_{eff} = \pi M^2(1-3P)+K_U$ denotes the effective uniaxial anisotropy constant. The first term in K_{eff} is due to the magnetostatic energy of perpendicularly-arrayed NWs [75-76] and constant, K_u, takes into account some additional second-order uniaxial anisotropy with the symmetry axis along wire direction [72]. The packing factor is defined as $P = \left(\pi d^2/2\sqrt{3}\,r^2\right)$ for a perfectly ordered hcp nanowire array. Consequently, it is expected that K_{eff} decreases linearly with P and finally the preferred axis of magnetization aligns in the transverse (i.e. perpendicular-to-wire-axis) direction for thicker NWs having high P. The equilibrium values of the polar angle (θ) for the magnetization vector $\vec{M}$ were obtained from static equilibrium conditions:

$$\begin{aligned} &E_\theta = \partial E/\partial\theta = 0 \\ &MH\begin{pmatrix}\cos\theta\sin\theta_H\cos(\phi-\phi_H)\\ -\sin\theta\cos\theta_H\end{pmatrix} - K_{eff}\sin^2\theta = 0 \end{aligned} \tag{2}$$

The resonance field values as a function of external field and magnetization angles were extracted from the dispersion relation in Eq. (3), derived via the Landau-Lifshitz dynamical equation of motion for magnetization with the Bloch-Bloembergen damping term [77-83],

$$\left(\frac{\omega_0}{\gamma}\right)^2-\left(\frac{1}{\gamma^2 T_2}\right)^2=\begin{pmatrix}\left(H\cos(\theta-\theta_H)+H_{eff}\cos 2\theta\right)\\ \times\left(H\cos(\theta-\theta_H)+H_{eff}\cos^2\theta\right)\end{pmatrix}. \qquad (3)$$

Here $(\omega_0/\gamma)=g\mu_B H$ is the Larmor frequency of the magnetization in the external *dc* effective magnetic field and $H_{eff}=2\pi M_S(1-3P)+(2K_u/M_s)$, which is the effective anisotropy field derived from the total magnetic anisotropy energy of NWs given in Eq. (1). The values of total magnetization were obtained by fitting H_{eff} to the experimental FMR data collected at different angles (θ_H) of external field $\vec{H}$. The experimental spectra are proportional to the derivative of the absorbed power with respect to the applied field which is also proportional to the imaginary part of the magnetic susceptibility. The theoretical absorption curves can be obtained by using $d\chi_2/dH$ (see Refs. 84-89 for details) where;

$$\chi=\chi_1+i\chi_2$$
$$\chi_2=\frac{\left(2\omega/\gamma^2T_2\right)}{\left((\omega_0/\gamma)^2-(\omega/\gamma)^2\right)^2+\left(2\omega/\gamma^2T_2\right)^2} \qquad (4)$$

with T_2 corresponding to the spin-spin relaxation time for the magnetization. This term contributes to the FMR line-width on the maximum of the derivative of absorption. $\omega=\gamma H$ represents the Larmor frequency of the magnetization in the *dc* applied field where γ is a constant referred to as the gyromagnetic ratio, $\gamma=g(\mu_0 e/2m_e)$, with the $g-$value for an electron being $g_e=2{,}0023$. The magnetic parameters were finally extracted by fitting the experimental spectra and their resonance field using Eqs. (3) and (4)

4. Results and Discussions

Fig. 3 shows the evolution of representative FMR spectra of Ni NWs in AAO and PCTE templates with Cu and Au substrates for selected angles. Similar FMR spectra and data were obtained for the Co NWs produced similarly (not shown). From these FMR spectra, the easy axis for all samples appears to be perpendicular to the wire axis, i.e. aligned in the NWs film plane. When the applied field is parallel to the wire axis, the spectra become asymmetric with respect to the resonance field. The spectra apparently contain two peaks near the applied field parallel to the wire axis region. While the main one corresponds to the bulk mode, the smaller one can be attributed to a surface mode due to the large surface-to-volume ratio of the individual NWs. Seemingly these modes unify into a single peak as the external field is rotated towards the film plane (i.e. perpendicular to the wire axis). The surface spin wave mode (SWM) is expected to originate from the surface anisotropy of individual wires. The SWM of NWs grown on Au substrate is clearer to observe compared to those grown on the Cu substrate. This SWM behaviour probable depends on the Au substrate according to the Cu substrate. This SWM is narrow and asymmetric near the parallel to the wires.

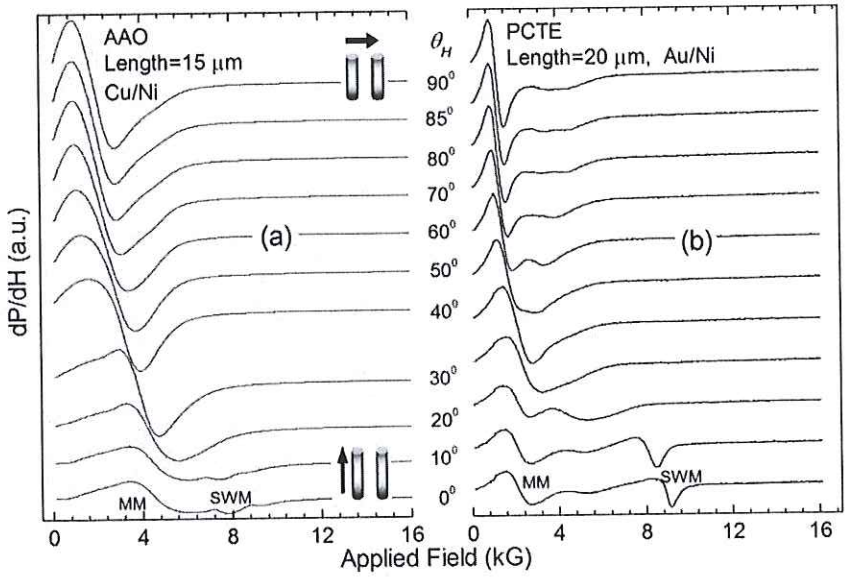

Fig. 3. Exemplary FMR spectra of two Ni NWAs given as function of the applied field direction. (**a**) Ni NWs ~ 40 nm diameter in an commercial AAO template (Whatman Anodics) with Cu substrate (sample1, S1). (**b**) Ni-NWs (200 nm diameter) in a PCTE template with Au substrate (sample4, S4).

Fig. 4 gives the evolution of the experimental (full circles) and calculated (full lines) resonance fields (H_r), along with the experimental resonance linewidth (open circles), as function of the applied field direction (θ_H) for different samples. The resonance field shows strongly anisotropic behavior with respect to the applied field direction. The extracted

magnetic parameters for all samples are reported in Table 1. The Ni NWs samples (S1 and S2), grown in AAO template using the Cu substrate, are observed to possess a single resonance field. Other Ni samples, namely S3 with AAO template and S4 with PCTE template, grown on the Au substrate, on the other hand, are observed have two resonance fields near the parallel-to-wire axis position (i.e. $\theta_H \approx 0$). Further, it can also be seen (by comparing S1 and S2) that H_r increases with the wire length when the template and substrate are the same. But, it can be seen from Figs. 4c and 4d that resonance field (H_r) increases by the PCTE template according to the AAO template. Here, wire length of NWs in PCTE template is smaller than nanowire in AAO template. The Ni-NWs in PCTE template is highly anisotropic compared to Ni-NWs in AAO template. From this result, highly anisotropic properties of Ni-NWs strongly depend on the substrates and templates. This anisotropic property originates from the interface between the Ni atoms and the Au substrate (Au atoms). It is found that the NWs possess dominant Ni texture on Au substrate.

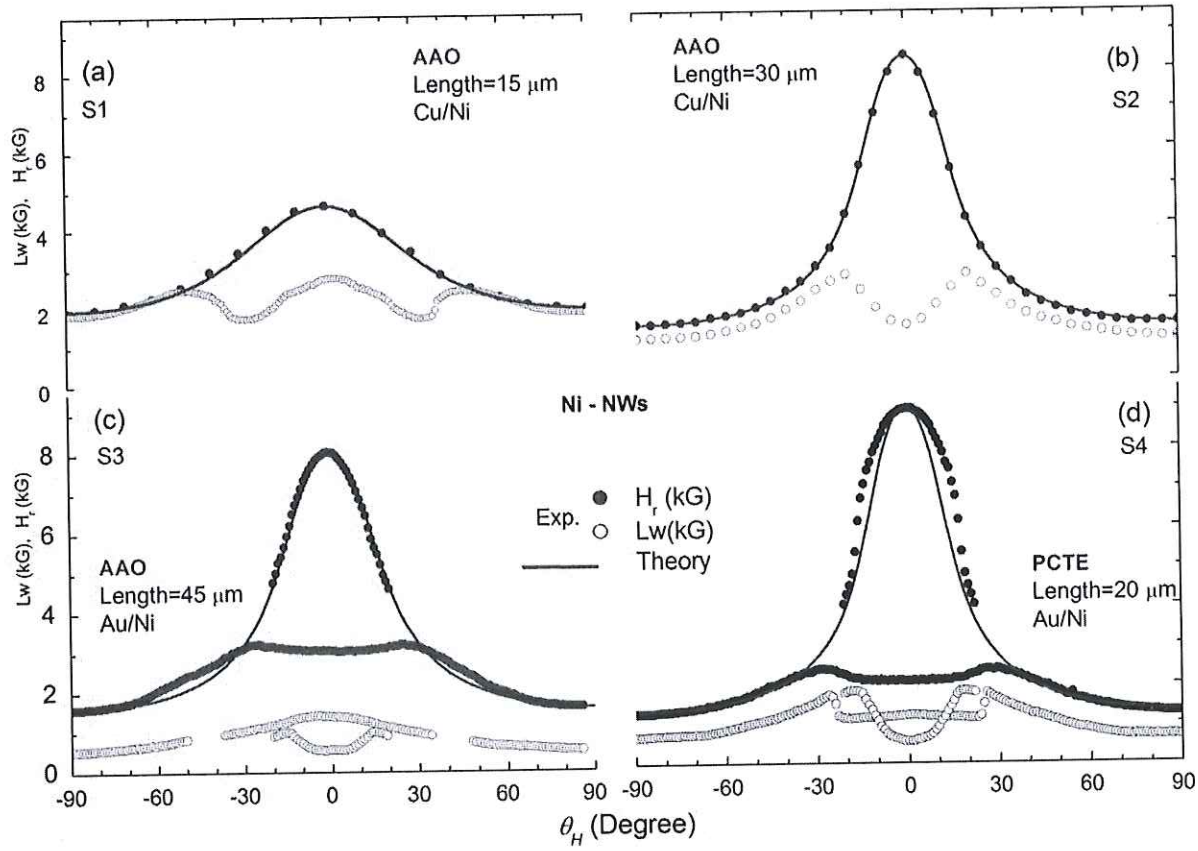

Fig.4. Experimental (full circles) and calculated (full red lines) resonance field and resonance linewidth (open circles) for Ni NWs of (**a, b**) the same substrate (Cu/Au) and template (AAO) and (**c, d**) different templates (AAO vs. PCTE) but the same substrate (Au).

Fig. 5 (a) shows the FMR spectra of two Co-NWs S5 grown in AAO template and S6 grown in PCTE template using the Cu substrate for parallel and perpendicular directions. The spectra

for the Co-NWs in AAO template were in general much broader and highly asymmetric (with respect to the resonance field) compared to the Co-NWs in PCTE template. The broadening of the Co-FMR spectra for NWs can be related to the magnetostatic interaction fields [69]. Details of the Co-NWs in the AAO template were given in Ref. 69. Consequently, near-neighboring Co wires in the AAO template are expected to be magnetized in antiparallel to the each other. Additionally, resonance behavior of the SWM may be observed in a multi-domain NWs [90]. The evolution of H_r (θ_H) for Co-NWs (S5) in AAO template and Co-NWs (S6) in PCTE templates are given in Fig. 5 (b). Moving from perpendicular to the parallel direction H_r increases for both samples. The H_r (θ_H) curve appears to be much broader and anisotropic for the Co-NWs in AAO template (S5). A good agreement exists between the experimental and theoretical angular dependence of resonance field of Co-NWs.

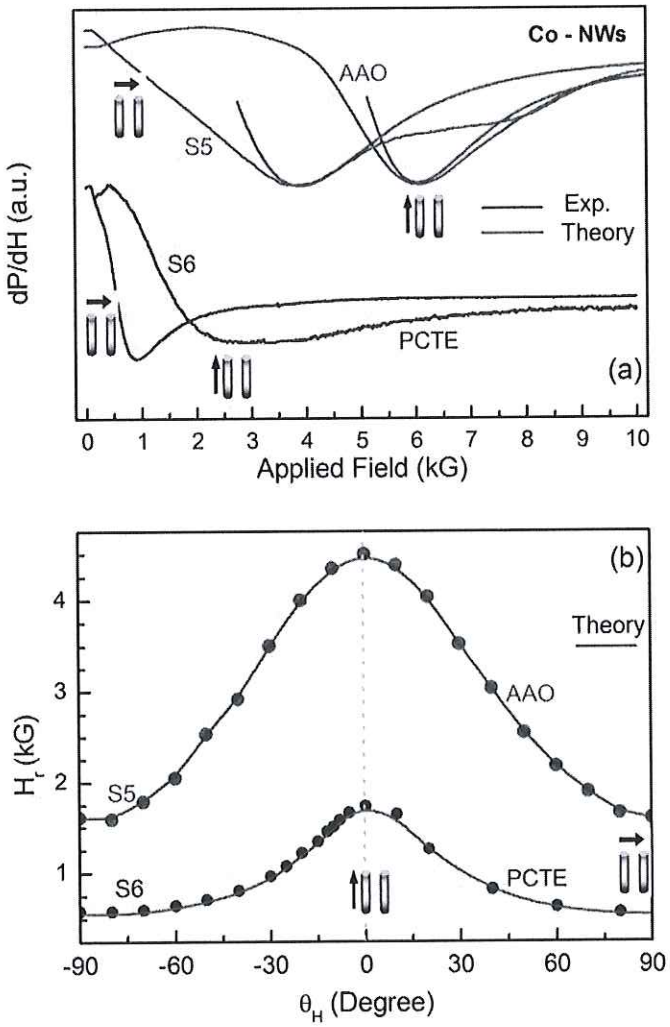

Fig.5. (**a**) Experimental and theoretical FMR spectra at parallel and perpendicular directions (with respect to the wire axis), and (**b**) angular dependence of the experimental (full green circle for Co-NWs in AAO template and full blue circle for Co-NWs in PCTE template) and theoretical (full red lines) resonance field as function of the applied field direction for Co-NWs in AAO and PCTE templates on the Cu substrate.

The calculated magnetic parameters of Ni and Co NWs are listed in Table 1. The uniaxial anisotropy parameters, Larmor frequency, g-values and spin-spin relaxation times for the magnetization were obtained by using the Eqs. (1), (3) and (4). The minimum and maximum uniaxial anisotropy values of 0.056×10^6 (erg/cm^3) and 0.147×10^6 (erg/cm^3) correspond to S1 and S4 for Ni-NWs, respectively. The uniaxial anisotropy value of S3 is 0.147×10^6 (erg/cm^3). This values nearly the same as S4. From this result, the pure Au substrate is effective for anisotropy for NWs. The maximum uniaxial anisotropy value for Co-NWs is 0.104×10^6 (erg/cm^3). At this point, template effect is important for anisotropy and other parameters. The Au substrate according to the Cu substrate has been widely assessing the anisotropy and Larmor frequency effects on Ni NWs.

Table 1. Calculated magnetic parameters for Ni and Co-NWs investigated in this work (diameter of samples is ~ 200 nm).

Sample No	Sample Name	L (μm)	Substrate	Template	$-K_u$ (erg/cm^3)$\times 10^6$	ω/γ (G)	g-value	$T_2 \times 10^{-7}$ (s)
S1	Ni	15	Cu	AAO	0.056	2750	3.32	3±0.5
S2	Ni	30	Cu	AAO	0.131	3050	3.003	4±0.5
S3	Ni	45	Au	AAO	0.139	3200	2.860	4±0.5
S4	Ni	20	Au	PCTE	0.147	3080	2.964	4±0.5
S5	Co	20	Cu	AAO	0.104	3150	2.905	1±0.5
S6	Co	12	Cu	PCTE	0.040	2850	3.211	1±0.5

The effective g-values of all samples is calculated from the scope of curve and found as g = 3.32, 3.003, 2.860, 2.964, 2.905, and 3.211 for S1, S2, S3, S4, S5, and S6, respectively. The g-factor is directly related to the ratio of the orbital and spin moment. In consideration of the spin-orbit interaction in magnetic NWs, part of the orbital moment can be pulled in the spin direction. If this interaction prefers the orbit and spin to be parallel to each other, the total magnetic moment will only be bigger than part of the spinel side and so g-factor will be bigger than free electron g-value 2.0023, Ni metallic g-value 2.18 and Co metallic g-value 2.17.

5. Conclusion

In this paper, Ni and Co NWs grown in commercial (Whatman anodisc) alumina (AAO) and polycarbonate membrane (PCTE) templates using gold (Au) and copper (Cu) substrates have been investigated for their magnetic properties via the ferromagnetic resonance (FMR)

technique. The FMR spectra, their resonance field and linewidth values to analyze the data collected were studied in the out-of-plane orientation (i.e. field parallel to NWs axis) in detail. There is no in-plane anisotropic behavior for FMR spectra at RT. The experimental FMR spectra, angular dependence of FMR resonance field, and their theoretical calculations are in a good agreement as well. The main resonance modes were broad according to the asymmetric SWM. The SWM were clearly observed in some cases and discussed relation to wire shape anisotropy for Ni and Co NWs. It is shown that SWM for Ni-NWs grown on pure Au substrate clearly appear in contrast to those grown on Cu bilayer substrate near the parallel-to-the-wire-axis condition. Furthermore, the SWM were generally observed only at low temperatures in literature. This work, however, appears to the first study in literature which reported SWM from magnetic NWs at the RT. The SWM for Ni-NWs in PCTE templates were observed in the high field region compared to those in AAO templates. The SWM is strongly dependent on substrate at RT. In other words, substrate for the SWM is effective than template on NWs.

Overall, the NWs indicated that an easy axis of magnetization that is perpendicular to the wire axis. This behavior originates from a competition between the shape anisotropy and dipolar/magnetostatic interactions. The wire diameter and shape dependence of the FMR spectra and SWM for Co-NWs produced in AAO templates show remarkable but complex distributions which deserve further study. The magnetic anisotropy and their relative importance are expected to the increase with Au substrate. In this work, our result is compatible with the result of Min et al. [91].

The effective *g*-values for all samples are bigger than the free electron *g*-value (2.0023). The *g*-values are directly related to the ratio of the spin and orbital moment. In consideration of the spin-orbit interaction, part of the orbital moment may be pulled in the spin orientation in magnetic nanowire arrays. If the spin-orbit interaction prefers the spin and orbit to be parallel to each other, the total magnetic moment of the magnetic nanowire arrays will only bigger than part of the spinel side and so *g*-values for all samples will be bigger than free electron *g*-value.

Acknowledgement

The support of the Scientific and Technological Research Council of Turkey (TUBİTAK) for project 107T635 is gratefully acknowledged.

References

[1] Giray Kartopu and Orhan Yalçın (2010). Fabrication and Applications of Metal Nanowire Arrays Electrodeposited in Ordered Porous Templates, Electrodeposited Nanowires and their Applications, Nicoleta Lupu (Ed.), ISBN: 978–953–7619–88–6, INTECH, Available from: http://sciyo.com/articles/show/title/fabrication-and-applications-of-metal-nanowire-arrays-electrodeposited-in-ordered-porous-templates.

[2] S. Sun, C. B. Murray, D. Weller, L. Folks, A. Moser, Science **287** (2000) 1989-1992.

[3] T.M. Whitney, J.S. Jiang, P.C. Searson, C.L. Chien, Science **261** (1993) 1318-1325.

[4] O. Yalçın (Ed.), Nanorods,ISBN:978-953-51-0209-0, Hard cover, InTech, Published: March 09, 2012 under CC BY 3.0 license, in subject Nanotechnology and Nanomaterials, 250 p., doi:10.5772/2046.

[5] Ordered Porous Nanostructures and Applications, ed. by R. B. Wehrspohn, Springer, 2005.

[6] L. Sun, Y. Hao, C.-L, Chien, P.C. Searson, IBM J. Res. Dev. **49** (2005) 79-102.

[7] G. Kartopu, O. Yalçın, K.-L. Choy, R. Topkaya, S. Kazan, and B. Aktaş, J. Appl. Phys. **109** (2011) 033909(1)-033909(8).

[8] S. Chui, Z. Lin, L. Hu, Phys. Lett. A **319** (2003) 85-88.

[9] C. Ramos, M. Vasquez, K. Nielsch, K. Pirota, J. Rivas, R. Wehrspohn, M. Tovar, R. Sanchez, U. Gösele, J. Magn. Magn. Mater. **272–276** (2004) 1652-1653.

[10] S. Melle, J. Menendez, G. Armelles, D. Navas, M. Vasquez, K. Nielsch, R. Wehrspohn, U. Gösele, Appl. Phys. Lett. **83** (2003) 4547-4549.

[11] G. Sauer, G. Brehm, S. Schneider, H. Graener, G. Seifert, K. Nielsch, J. Choi, P. Göring, U. Gösele, P. Miclea, R. B. Wehrspohn, Appl. Phys. Lett. **88** (2006) 023106(1)-023106(3).

[12] K.-H. Xue, G.-P. Pana, M.-H. Panb, M. Lub, G.-H. Wang, Superlattices and Microstructures **33** (2003) 119-129.

[13] P.Y.-Tao, M.G.-Wen, S.W.-Jun, F. Qui, Z.L.-De, Chinese Phys. Lett. **20** (2003) 144-147.

[14] B. Yoo, Y. Rheem, , W.P. Beyermann, N.V. Myung, Nanotechnology **17** (2006) 2512-2517.

[15] S. Karim, K. Maaz, Mater. Chem. Phys. **130** (2011) 1103-1108.

[16] G. Kartopu, O. Yalçın, M. Es-Souni, A. C. Başaran, Appl. Phys. **103** (2008) 093915(1)-093915(6).

[17] L. Cattaneo, S. Franz, F. Albertini, P. Ranzieri, A. Vicenzo, M. Bestetti, P.L. Cavallotti, Electrochimica Acta **85** (2012) 57-65.

[18] G. Ji, Z. Gonga, Y. Liu, X. Changa, Y. Dub, M. Qamar, Solid State Commun. **151** (2011) 1151-1155.

[19] X. Lin, G. Ji, T. Gao, X. Chang, Y. Liu, H. Zhang, Y. Du, Solid State Commun. **151** (2011) 1708-1711.

[20] R. Lavín, C. Gallardo, J.L. Palma, J. Escrig, J.C. Denardin, J. Magn. Magn. Mater. **324** (2012) 2360-2362.

[21] Gui-Fang Huang, Wei-Qing Huang, Ling-Ling Wang, B.S. Zou, A. Pan, Journal of Magnetism and Magnetic Materials **324** (2012) P. 4043.

[22] B. Das, K. Mandal, P. Sen, A. Bakshi, P. Das, Physica B **407** (2012) P. 3767.

[23] T.S. Ramulu, R. Venu, S. Anandakumar, V. Sudha Rani, S.S. Yoon, C.G. Kim, Thin Solid Films **520** (2012) 5508-5511.

[24] A. Ramazani, M.A. Kashi, G. Seyedi, J. Magn. Magn. Mater.**324** (2012) 1826-1831.

[25] A.P. Chumakov, S.V. Grigoriev, N.A. Grigoryeva, K.S. Napolskii, A.A. Eliseev, I.V. Roslyakov, A.I. Okorokov, H. Eckerlebe, Physica B **406** (2011) 2405-2408.

[26] B. Kalska-Szostko, E. Orzechowska, Curr. Appl. Phys. **11** (2011) S103-S108.

[27] M. Darques, L. Piraux, A. Encinas, Ieee Trans. Magn. **41** (2005) 3415-3417.

[28] A. Sklyuyev, M. Ciureanu, C. Akyel, P. Ciureanu, A. Yelon, J. Appl. Phys. **105** (2009) 023914(1)-023914(8).

[29] Y. Zhang, G.S. Chaubey, C. Rong, Y. Ding, N. Poudyal, Po-ching Tsai, Q. Zhang, J.P. Liu, J. Magn. Magn. Mater. **323** (2011) 1495-1500.

[30] F. Vidal, P. Schio, N. Keller, Y. Zheng, D. Demaille, F.J. Bonilla, J. Milano, A.J.A. de Oliveira, Physica B **407** (2012) 3070-3073.

[31] Z. Song, Y. Xie, S. Yao, H. Wang, Materials Letters **65** (2011) 44-45.

[32] S. Wedekind, F. Donati, H. Oka, G. Rodary, D. Sander, J. Kirschner, Surface Science **606** (2012) 1577-1580.

[33] E. Mafakheri, P. Tahmasebi, D. Ghanbari, Measurement **45** (2012) 1387-1395.

[34] Z. Wei, Z. Ye, K.D.D. Rathnayaka, I.F. Lyuksyutov, W. Wu, D.G. Naugle, Physica C **479** (2012) 41-44.

[35] X.W. Wang, Z.H. Yuan, H.F. Luo, Solid State Sci. **13** (2011) 1211-1214.

[36] V. Scarani, H.De Riedmatten, J.-P. Ansermet, Appl. Phys. Lett. **76** (2000) 903-905.

[37] M. Darques, Anne-Sophie Bogaert, F. Elhoussine, S. Michotte, J. de la T. Medina, A. Encinas, L. Piraux, J. Phys. D, Appl. Phys. **39** (2006) 5025-5032.

[38] S. Y. Chou, P. R. Krauss, and P. J. Renstrom, Science **272** (1996) 85-87.
[39] A. Ramazani, M.A. Kashi, S. Kabiri, M. Zanguri, Journal of Crystal Growth **327** (2011) 78-83.
[40] A. Ramazani, M.A. Kashi, S. Ghanbari, F. Eshaghi, J. Magn. Magn. Mater. **324** (2012) 3193-3198.
[41] S. Pal, S. Saha, D. Polley, A. Barman, Solid State Commun. **151** (2011) 1994-1998.
[42] M. Darques, L. Piraux, A. Encinas, P. B.-Guillemaud, A. Popa, U. Ebels, Appl. Phys. Lett. **86** (2005) 072508(1)- 072508(3).
[43] G. Ferrara, C. Arbizzani, L. Damen, M. Guidotti, M. Lazzari, F.G. Vergottini, R. Inguanta, S. Piazza, C. Sunseri, M. Mastragostino, J. Pow. Sour. **211** (2012) 103-107.
[44] L.-P. Carignan, V. Boucher, T. Kodera, C. Caloz, A. Yelon, D. Ménard, Applied Physics Letters **95** (2009) 062504(1)- 062504(3).
[45] International Workshop on Magnetic Wires, San Sebastian, Spain, J. Magn. Magn. Mater. **249** (2002) 146-155.
[46] R. O'Barr, S.Y. Yamamoto, S. Schultz, W. Xu, A. Scherer, J.Appl. Phys. **81** (1997) 4730-4732.
[47] R. Skomski, H. Zeng, M. Zheng, D. J. Sellmyer, Phys. Rev. B **62** (2000) 3900-3904.
[48] S. H. Xue, Z. D. Wang, Mater. Sci. Eng. B **135** (2006) 74-77.
[49] P. Evans, W.R. Hendren, R Atkinson, G.A. Wurtz, W. Dickson, A.V. Zayats, R.J. Pollard, Nanotechnology **17** (2006) 5746-5753.
[50] K. Nielsch, R.B. Wehrspohn, J. Barthel, J. Kirschner, U. Gösele, App. Phy. Lett. **79** (2001) 1360-1362.
[51] H. Zeng, R. Skomski, L. Menon, Y. Liu, S. Bandyopadhyay, D.J. Sellmyer, Phys. Rev. B **65** (2002) 134426(1)- 134426(8).
[52] G. Kartopu, O. Yalçın, K.-L. Choy, R. Topkaya, S. Kazan, B. Aktaş, J. Appl. Phys. **109** (2011) 033909(1)-033909(8).
[53] P. E. Wigen, Thin Solid Films **114** (1984) 135-186.
[54] G. Kartopu, O. Yalçın, S. Kazan, M. Es-souni, B. Aktaş, J. Magn. Magn. Mater. **321** (2009) 1142-1147.
[55] U. Ebels, J.-L Duvail, P.E. Wigen, L. Piraux, L.D. Buda, K. Ounadjela Phys. Rev. B **64** (2001) 144421(1)-144421(6).
[56] M. Darques, L. Piraux, A. Encinas, P.B.-Guillemaud, A. Popa, U. Ebels, Appl. Phys. Lett. **86** (2005) 072508(1)- 072508(3).
[57] J.D.L.T. Medina, L. Piraux, J.M.O. Govea, A. Encinas, Phys. Rev. B **81**, (2010) 144411(1)-144411(11).
[58] B. Aktaş, and M. Özdemir. Physica B **119** (1994) 125-138.
[59] B. Aktaş, Solid State Commun. **87** (1993) 1067-1071.
[60] R.B. Morgunov, A.I. Dmitriev, Y. Tanimoto, J.S. Kulkarni, J.D. Holmes, O.L. Kazakova, Physics of the Solid State Vol. **50** (2008) 1103-1109.
[61] B. Aktaş, B. Heinrich, G. Woltersdorf, R. Urban, L. R. Tagirov, F. Yıldız, K. Özdoğan, M. Özdemir, O. Yalçın, and B. Z. Rameev, J. Appl. Phys, **102** (2007) 013912(1)- 013912(8).
[62] B. Aktaş, Solid State Commun. 87 (1993) 1067-1071.
[63] B. Aktaş, M. Özdemir, Physica B: Condensed Matter 193 (1994) 125-138.
[64] H. Masuda, K. Fukuda, Science, **268** (1995) 1466-1468.
[65] D. AlMawlawi, N. Coombs, M. Moskovits, J. Appl. Phys. **70** (1991) 4421-4425.
[66] Y. Henry, K. Ounadjela, L. Piraux, S. Dubois, J.–M. George, J.-L. Duvail, Eur. Phys. J. B **20** (2001) 35-54.
[67] R. Yong, W.J.-Bo, L.Q.-Fang, H.X.-Hua, X.D.-Sheng, Chinese Phys. B **18** (2009) 3573-3576.
[68] F.Nasirpouri Transworld Research Network 37/661 (2007) 2-37.
[69] G. Kartopu, O. Yalçın, S. Kazan, B. Aktaş, J. Magn. Magn. Mater. **321** (2009) 1142-1147.
[70] G. Kartopu, M.E. -Souni, A.V. Sapelkin, D. Dunstan, Phys. Stat. Solidi (a) **203** (2006) R82-R84.
[71] G. Kartopu, M. E. -Souni, A.V.Sapelkin, D. Dunstan, J. Nanosci. Nanotechnol. **8** (2008) 931-935.
[72] A.E. -Oropesa, M. Demand, L. Piraux, I. Huynen, U. Ebels. Phys. Rev. B **63** (2001) 104415(1)-104415(6).
[73] A. Encinas-Oropesa, M. Demand, L. Piraux, U. Ebels, and I. Huynen. J. Appl. Phys. **89** (2001) 6704-6706.
[74] A. Encinas, M. Demand, L. Vila, L. Piraux, App. Phys. Lett. **81** (2002) 2032-2034.
[75] M. Demand, A. E. -Oropesa, S. Kenane, U. Ebels, I. Huynen, L. Pirax. J. Magn. Magn. Mater. **249** (2002) 228-233.
[76] J. Dubowik. Phys. Rev. B **54** (1996) 1088-1091.
[77] O. Yalçın, F. Yıldız, M. Özdemir, B. Aktaş, Y. Köseoğlu, M. Bal, M.T. Touminen. J. Magn. Magn. Mater. **272-276** (2004) 1684-1685.
[78] O. Yalçın, S. Kazan, R. Şahingöz, F. Yildiz, Y. Yerli, B. Aktaş, J. Nanosci. Nanotech. **8** (2008) 841-845.
[79] S. Güner, O. Yalçın, S. Kazan, F. Yıldız, R. Şahingöz, Phys. Stat. Solid (a) **203** (2006) 1539-1544.
[80] B. Aktaş, Thin Solid Films, **307** (1997) 250-259.
[81] A.A. Stashkevich, Y. Roussigné, P. Djemia, S.M. Chérif, P.R. Evans, A.P. Murphy, W.R. Hendren, R. Atkinson, R.J. Pollard, A.V. Zayats, G. Chaboussant, F. Ott, Phys. Rev. B **80** (2009) 144406(1)-144406(13).
[82] A. Kharmouche, J. Ben Youssef, A. Layadi, and S.-M. Chérif, J. App. Phys. **101** (2007) 113910(1)-

113910(6).
[83] O. Yalçın, F. Yıldız, B. Z. Rameev, M.T. Tuominen, M. Bal, M. Özdemir, B. Aktaş. Nanostructured Magnetic Materials and their Applications. Kluwer Academic Publisher. Nato Science Series. **143** (2004) 345-356.
[84] J.H. Min, J.U. Cho, Y.K. Kim, J.-H. Wu, Y.-D. Ko, J.-S. Chung, J. Appl. Phys. **99** (2006) 08Q510(1)-08Q510(2).
[85] Y. Öner, M. Özdemir, B. Aktaş, C. Topacli, E. A. Haris, S. Senoussi, J. Magn. Magn. Mater. **170** (1997) 129-142.
[86] B.D. Cullity, C.D. Graham, Introduction to Magnetic Materials, Wiley p. 199 (2009).
[87] B. Aktaş, Thin Solid Films **307** (1997) 250-259.
[88] B. Aktaş, M. Özdemir, R. Yilgin, Y. Öner, T. Sato, T. Ando, Physica B **305** (2001) 298-314.
[89] B. Aktaş, F. Yildiz, B. Rameev, R. Khaibullin, L. Tagirov, M. Özdemir, Physica status solidi (c) **12** (2004) 3319-3323.
[90] H. Xi, S. Xue, J. App. Phys. **101** (2007) 123905(1)-123905(6).
[91] J. H. Min, J. U. Cho, Y. K. Kim J. Appl. Phys. **99** (2006) 08Q510(1)-08Q510(2).